INFORMATION EXTRACTION TECHNIQUES FOR MULTISPECTRAL SCANNER DATA

by

William A. Malila, Robert B. Crane,
Wyman Richardson, Robert E. Turner
Willow Run Laboratories
The University of Michigan
Ann Arbor, Michigan

INTRODUCTION

This paper summarizes some of the work during 1971 at the Willow Run Laboratories that has been directed toward four information extraction problems: (1) signature extension for improved recognition processing over large areas, (2) the choice of density functions for recognition decision rules, (3) channel selection for cost reduction, and (4) radiation balance mapping for interpretation of wide-spectrum scanner data. The details of these studies are reported in References 1 and 2.

Signature extension and cost reduction are problems that must be solved if the promise of large-area surveys of Earth resources and man's impact on his environment are to be realized. The techniques presently in use are limited in their ability to provide recognition and other information extraction with sufficient accuracy, timeliness, and cost effectiveness to make operational uses a practical reality. These techniques should be improved and refined for use on data from both aircraft and spacecraft.

A two-pronged approach is being followed in the development of techniques to overcome the degradation of recognition accuracy that occurs because systematic variations in scanner data cause the signatures obtained from training areas to be different from data collected farther in time and/or space from the training areas. The first is a theoretical approach to examine the sources of variation in scanner data and gain insight for improved techniques by the simulation of scanner radiance signals. The second is a more empirical approach for the development of preprocessing techniques to remove systematic effects from scanner data so that large areas can be surveyed accurately with a minimum of ground-truth information.

Preprocessing has been under development at Michigan as one method for removing systematic effects from scanner data before recognition processing (Fig. 1). During last year's meeting, Mr. Legault discussed some of the methods that we have explored [3]. These include the transformation of data (such as by ratioing signals), the use of data from a sky sensor on

the aircraft, and the use of in-scene reference areas to develop corrections for signature extension. At Michigan, preprocessing was used during 1971 in the processing and analysis of Corn Blight data [4] and in data processing tasks for various users [5]. In this paper, a generalized preprocessing technique that has been developed and tested during 1971 is discussed [1,6].

Multispectral recognition decision rules use likelihood functions of the various material classes. Our second area was an investigation into the suitability of the normal (Gaussian) likelihood functions for these decision rules as opposed to empirical likelihood functions.

In the third problem area, cost reduction, we improved our procedures for selecting a subset of channels or features for use in the recognition processor. Our digital channel selection procedures use a criterion that can be formulated as an average probability of misclassification, a quantity with direct physical interpretation. Our most exact procedure is time consuming and this negates some of the cost advantage gained by reducing the number of processing channels. However, we have recently developed a much faster method by making use of a linear approximation in our calculations.

In the fourth area, we endeavor to use the full spectrum of scanners for interpretation aspects of multispectral remote sensing. Energy budgets are of interest in many studies of natural and agricultural areas, and they also are being used increasingly in urban studies. Since net radiation is the most important component of an energy budget and the scanner measures the apparent outgoing radiation, procedures for producing maps of the outgoing radiation, and the net radiation or radiation balance were developed and applied.

EXAMINATION OF SYSTEMATIC VARIATIONS BY SIMULATION

Figure 2 lists some sources of variation in multispectral scanner signals that are associated with conditions of measurement (such as atmospheric haze and the position of the sun) and parameters of measurement (such as the scan geometry and the sensor characteristics). Although not listed, there also are variations associated with the characteristics of the surface materials being observed, such as inhomogeneities and bidirectional reflectance characteristics. While both systematic and random variations are listed, the systematic variations are the ones that most seriously reduce the recognition accuracy away from the training areas.

Last year, a theoretical radiative transfer model was developed at Michigan to simulate multispectral scanner signals [7]. This model characterizes the spatial and spectral distribution of radiation in Earth's atmosphere as a function of several parameters and conditions of measurement. During the past year, the model was improved, extended, and used to simulate scanner radiance signals and other radiometric quantities and their systematic variations under a wide variety of conditions [1,8].

One of the major improvements made in the model was the incorporation of time as an independent parameter which allows us to simulate temporal variations that would be present in area survey data. Another is the use of exact scattering phase functions in our calculation procedure which has increased the accuracy to the point where our calculations agree well with measurements of sky radiance and with theoretically exact calculations based on Chandrasekhar's theory.

The next nine figures present graphs that are representative of the model's ouput and illustrate the sources of systematic variation in scanner data. Figure 3 shows the dependence of transmittance on scan angle for four different visual ranges. V=2 km corresponds to a dense haze and V=23 km represents a normal clear day (bordering on a light haze). The airborne scanners generally collect data at scan angles of ±45° or smaller, and it is clear that the path transmittance for these angles varies substantially. The transmittance and all other quantities depend on the altitude of the observer, and the data in this figure are for an altitude of 3 km. While all of the data presented herein are for aircraft altitudes, the model also can be used to simulate data collected from spacecraft.

Irradiance is another quantity of interest. Figure 4 shows the spectrum of the irradiance that would be detected by a sky sensor on an aircraft flying at an altitude of 1 km. Note the increase in levels for the hazy condition, that is, for short visual ranges. Information of this sort is of value in using the sky sensor signals for signature extension.

Next consider the downlooking scanner. Not all the radiation that reaches the scanner originates at the surface element being viewed. There is a quantity called path radiance, which is extraneous radiation that is scattered into the field of view by the atmosphere.

Figure 5 shows that path radiance depends strongly on visual range and wavelength. The wavelength dependence is much different than that for the irradiance shown in Figure 4. The reason for this difference is that path radiance depends on the reflectance spectrum of the material being viewed. In this instance, the spectrum is that of green vegetation.

Path radiance also depends on the nadir scan angle and the location of the sun. Figure 6 shows the scan-angle dependence of path radiance for three different sun positions on a very hazy day. The scan plane includes the sun, and one readily can see the characteristic peak in backscattered radiance at the antisolar angle. When the scan plane does not include the sun, the path radiance is a much more symmetric function of scan angle. Figure 7 shows how path radiance would vary throughout one day if the aircraft were flying East or West at an altitude of 1 km on a medium hazy day. The scan is in the North-South plane. Note the increase and decrease of the radiance at any given scan angle as the time changes throughout the day. Also note the increase in path radiance at noon when the sun moves into the scan plane. This type of information is useful for planning flight lines.

A scanner measures the total radiance from the view direction; thus, the atmospheric effects of path radiance and transmittance are both present in its signals. Figure 8 simulates the total radiance that would be received by the scanner from a diffusely reflecting surface with the reflectance spectrum of green vegetation. A comparison of Figures 7 and 8 shows that the path radiance is a substantial component of the total received radiance. Both figures show the large and systematic changes in signal level that are associated with time of day, that is, with sun position.

Now, let us examine the scan angle dependence more closely. Figure 9 presents a comparison between experimental measurements of sky radiance and calculated values for three different surface albedos. Note the excellent agreement between the shapes of the experimental and the calculated curves of sky radiance. We also compared total radiance calculated with the model and total radiance measured by our scanner for several fields of soybeans. The data are presented in Figure 10. One immediately notes the difference in angular response. We believe that much of this difference is due to the surface reflectance characteristics. The simulation model assumed a perfectly diffuse, or Lambertian, surface, whereas results presented in this volume on reflectance modeling of corn [9] and results of other investigators show that agricultural crops, like soybeans, do have definite bidirectional reflectance characteristics. We are presently modifying our model to include such reflectances.

To complete this part of the discussion, two graphs that depict interdependencies of radiation quantities as functions of time of day are presented. Figure 11 presents the ratio of the total downward irradiance at an altitude of 5 km to the total irradiance at the Earth's surface. We see that the irradiance at the aircraft is slightly greater than on the ground, and becomes more so with an increase in haze below the aircraft. There is relatively little change in the ratio for two hours either side of solar noon when conditions are clear (V=23 km), but the time dependence for that interval increases for shorter visual ranges. In all cases, there is strong time dependence during early morning and late afternoon hours. This type of information can be helpful in using sky sensor signals for signature extension.

The second interdependence, presented in Figure 12, is the ratio of path radiance to total radiance. These curves clearly show that path radiance is a large fraction of the total radiance, especially for very hazy conditions. The important point of Figure 12 is that, for reasonably clear days, the ratio of path radiance to total radiance is essentially constant for several hours at mid-day for a given atmospheric condition and a fixed surface albedo. This fact should be of value in the development of techniques to remove atmospheric effects from data. It is worth noting that the difference between atmospheric effects at an altitude of 5 km and at low altitude is greater than between 5 km and space altitudes.

TECHNIQUES FOR OVERCOMING SYSTEMATIC VARIATIONS

The simple physical model that has been used in our analysis is as follows:

$$L(\theta, i, j) = \rho'_{ij} E_j(\theta) T_j(\theta) + L_{pj}(\theta) + L_{nj} \qquad (1)$$

where L is the radiance signal,
i denotes the class of ground cover being scanned,
j denotes the spectral channel,
θ is a vector that describes the parameters and conditions of the measurement,
ρ'_{ij} is the bidirectional reflectance of the surface (for a diffuse surface, $\rho'_{ij} = \rho_{ij}/\pi$, where ρ_{ij} is the diffuse or directional reflectance),
E_j is the irradiance in channel j,
T_j is the corresponding atmospheric transmittance,
L_{pj} is the path radiance in channel j, and
L_{nj} is the noise-equivalent radiance in channel j.

Equation (1) has exact physical meaning only when the reflectance of the surface is diffuse and, consequently, has no angular dependence. However, for preprocessing, one can define a generalization in which angular dependence is allowed.

As can be seen in Equation (1), the atmosphere contributes both an additive term, L_p, the path radiance, and a multiplicative term, T, the transmittance. From this, we conclude that, in general, a preprocessing transformation should include both additive and multiplicative correction functions. Our general preprocessing transformation, called the U-V transformation, meets this requirement.

The operating principle of this transformation is one of adjusting a signal, $L(\theta)$ to $L(\theta_o)$, the value it would have had, had it been measured under a reference set of conditions represented by θ_o. That is,

$$L(\theta_o) = L(\theta)U(\theta) + V(\theta) \qquad (2)$$

where $L(\theta_o)$ is the radiance at reference condition, θ_o,
θ is a vector quantity that denotes conditions and parameters of measurement, and
$U(\theta)$ and $V(\theta)$ are correction functions that are independent of the material classes.

Clearly, $V(\theta)$ is the additive correction function and $U(\theta)$ is the multiplicative one.

There are several systematic or deterministic effects for which the technique potentially can correct; these include scan angle effects, illumination changes along the flight line, cloud shadows, altitude effects, and day-to-day changes in conditions. We will discuss and show examples of corrections only for scan angle effects and altitude effects.

The correction functions, $U(\theta)$ and $V(\theta)$, can be determined either from the data or from model calculations. The simplest empirical procedure for scan angle correction is to select two relatively uniform fields of different reflectance that extend over a common range of scan angles. The solution of simultaneous equations yields the U and V functions. More general ways have been developed and applied.

We determined angle correction function for a data set collected under hazy conditions (at a visual range of $\sim$6 km). Figure 13 presents plots of average signal vs. scan angle for six soybean fields before angle correction was applied. The data cover a scan angle interval roughly $\pm 25°$ from nadir. Even though the ordinate scale accentuates differences, a substantial scan angle effect is evident in all fields. These within-field angle variations mask the between-field differences present in this data set. Figure 14 shows the same six fields after U-V angle corrections were applied. The within-field angle variations have now been reduced to the point where the between-field differences dominate the data set.

An indirect method for testing the ability of preprocessing techniques to remove systematic variations is to perform recognition on data sets with and without preprocessing. Differences between fields used for training and those in other parts of the data set, however, can mask or obscure the improvements produced by the techniques in such a test.

Figure 15 presents a comparison of recognition errors for different treatments of the data sets where, like golf, the smaller numbers signify better performance. The left-hand three data columns are for data collected at an altitude of 1,000 ft and processed with training areas selected from within that data set. The first column gives recognition errors without data smoothing and without preprocessing. The fact that 48% of the fields had less than half their elements identified correctly is a feature of the data set and the way in which the training areas were selected. Only 14% of the fields were incorrectly classified when the majority decision was assigned to the field. As shown in the second column, a smoothing to reduce system noise and element-to-element variation did not appreciably affect the recognition performance here, although it has been useful in other instances. Then, when we examine column 3, we see that the application of the U-V preprocessing transformation produced a substantial reduction in classification errors according to both criteria.

The two columns on the right of Figure 15 represent data collected at an altitude of 5,000 ft. The first of the two used training areas from the 5,000-ft data and no preprocessing. The second used the U-V preprocessing transformation in two ways, one to remove scan angle effects and one to extend training signatures from 1,000 ft to 5,000 ft. The recognition errors resulting from use of 1,000-ft signatures are comparable with those for 5,000-ft signatures. Although the comparison would be less favorable had the 5,000-ft data been preprocessed, the signature extension demonstration is still encouraging.

SUITABILITY OF THE NORMAL LIKELIHOOD FUNCTION FOR RECOGNITION DECISION RULES

Likelihood functions are used in classification decision (i.e., recognition) processes on multispectral scanner data. These functions are usually represented by multivariate normal (Gaussian) density functions, whose statistical parameters are determined for the various decision classes from subsets of the data. Last year, we tested the normality of individual subsets of data corresponding to single fields, and all were found to be non-normal at the 1% level of significance using a standard chi-square goodness of fit test [7]. During the year just ended, we compared two maximum likelihood decision rules on the basis of paired receiver operating characteristic (ROC) curves, one member of each pair representing a multivariate normal decision rule and the other a rule based on an empirical density function. For each data set, an alternative hypothesis was assumed, and the Type I vs. Type II errors (probability of miss vs. false alarm) were plotted for different decision levels for each decision rule; see Figure 16 for a typical pair of ROC curves. From such curves a direct comparison can be made between the two likelihood function decision rules.

The choice of an alternative hypothesis is an important consideration. If we consider the data to be points in a hyperspace, of which each coordinate corresponds to a transformed spectral channel, then the question becomes one of: where in the hyperspace shall we locate the alternative hypothesis? The location and shape of the alternative distribution can be expected to affect the decision errors. A distribution was chosen that was uniformly located in the hyperspace and corresponds to the use of many different separate distributions located uniformly in the hyperspace. Thus, the results correspond to an average of the performance that would be obtained using a large number of separate distributions. This choice of an alternative distribution has the additional advantage of making it possible for one to test each data set individually.

The Type I errors were found by selecting a decision level and counting the percentage of points that were rejected by using first one, then

the other, decision rule. The Type II errors were found by direct calculation. Data points for the alternative were assumed to be located uniformly throughout a hyper-rectangular parallelepiped, the dimensions of which were set so that 0.9995 of the volume of the Gaussian distributions would be included.

As a result of our tests, we have decided that the use of the normal likelihood function for individual fields is justified for recognition processing of multispectral scanner data. This function is much quicker to generate and use than the histogram function. Also, the improvement in performance that would result from using a histogram likelihood function and all of the channels is not believed to be significant. More promising approaches, we believe, are (1) to preprocess the data to compensate for scan angle and similar systematic effects and/or (2) to compensate by changing the decision rule parameters. By using the first approach, we would expect the transformed data to have distributions that are more nearly normal and at the same time, have reduced variances.

CHANNEL SELECTION

Digital recognition processing costs are proportional to the square of the number of channels used for quadratic decision rules so a reduction in the number of channels reduces costs. Analog and hybrid systems can maintain a high throughput rate for any number of channels, but their flexibility and capacity for different material classes are reduced when many information channels are used for recognition.

The principal features of our channel selection procedure are listed in Figure 17. First, we have chosen the Bayesian criterion, average expected loss. It can be formulated as an average probability of misclassification and has a direct physical interpretation.

To make the calculation of this criterion practical, we have had to make a number of assumptions which are straightforward and have been analyzed and verified. First, we assume normal (Gaussian) statistics. Second, we use a pairwise method of calculation, and third, we use a stepwise procedure that successively adds the one channel which gives the lowest average probability of misclassification when used with those already selected.

Recently, we developed a much faster procedure that assumes a linear approximation to the quadratic decision surface which results in a much simpler calculation of the probability of misclassification. The new linear method is 50 times faster than the quadratic method, and its use results in substantial savings while retaining the interpretation feature of the older method. Figure 18 presents a comparison of results obtained with the two procedures for a data set with nine signatures and ten data channels. Note first the difference in time - one hour for the quadratic

method and only 70 seconds for the linear method. Next, we see that the ordering of the channels is the same in both cases for the first six channels. Finally, we see that the average probabilities of misclassification computed by the linear method are in very good agreement with those of the other method.

RADIATION BALANCE MAPPING

Our final study results from the fact that synchronous reflective and thermal data have become available. We now can explore an interpretive use of scanner data in analyzing the energy budgets of vegetation and other surface materials, both man-made and natural. An energy budget is simply a statement of the fact that materials maintained balance in the exchange of energy with their environment. As shown in Figure 19, there is a net amount of radiant energy absorbed by an object, like a plant, from its surroundings. This energy is partitioned into several components. The first component is used in evaporating water such as in transpiration. Other components heat the air around the plant and soil or represent energy conducted away from them. Finally, there is a net energy conversion component which usually is small by comparison. From this partitioning of net absorbed radiant energy, it is clear why net radiation is of interest for irrigation and water stress studies.

The instantaneous net rate at which radiant energy is absorbed by a surface also is made up of several components as shown in Figure 20. A fraction, ρ, of the short-wavelength irradiance, E_s, is reflected leaving a net amount absorbed equal to $(1 - \rho)E_s$. Next, there is a substantial amount of thermal radiation from the atmosphere and surroundings that is absorbed. Finally, the surface itself emits thermal radiation.

A multispectral scanner measures the outgoing radiance of a surface, in many channels, through the atmosphere. Figure 21 is a map of the apparent outgoing radiation or exitance from an agricultural area. It was produced by weighting and summing the contributions from the various scanner channels. The atmospheric effects (path radiance and transmittance) must be removed to obtain the actual exitance of each surface with the assumed spatial distribution of exitance. The small dark spots in the lower left hand corner are young trees in an orchard. The dark circular area above them is wet bare soil, surrounded by dry bare soil. Less radiation is leaving the wet soil because it is darker and because the energy used to evaporate the water keeps its temperature lower. At the right of the map, we have two corn fields; the lower one is darker; it was more mature, reflected less near-IR radiation, and had more evapotranspiration than the upper field.

Upon estimating the incoming power density at both short and long wavelengths, a map of net radiation or radiation balance can be produced and

would appear as shown in Figure 22. Here, the relative tones are reversed from those of the previous slide. The wet soil and vegetation which have the highest net radiation values are here displayed in light tones.

CONCLUDING REMARKS

Four aspects of techniques for extracting useful information from multispectral scanner data are discussed above. Our major emphasis is on the problems that have held back the use of scanner data for large-area surveys, for instance, problems of extending recognition performance away from areas used to train the recognition computers,

Sources of systematic variation have been examined by use of a simulation model and some valuable insights have been gained. These insights, through techniques based on the model calculations, will be applied to real scanner data during the coming year. The model is applicable to both aircraft and space data.

Preprocessing is one method for removing these systematic effects so as to improve recognition performance. We have developed a general technique and demonstrated its ability to reduce scan angle variations and to extend signatures from one altitude to another. We also have studied the extension of the technique to two dimensions and must now develop it to remove systematic variations that occur along the direction of flight as the sun changes position and atmospheric conditions change. This is an important problem for area survey operations.

While preprocessing is an efficient method for removing systematic variations, it transforms all signals in exactly the same way regardless of their material class. More flexibility in processing, such as the use of adaptive techniques, would be possible if the decision rule parameters were changed in addition to changing the data.

A study of the usefulness of empirical density functions as opposed to the normal (Gaussian) density function for recognition processing led to the conclusion that the normal assumption for individual fields is justified for processing multispectral scanner data,

We have developed a rapid method for choosing subsets of information channels to use for processing. While thus far it has been applied only for selecting among scanner channels, it can be used to select among other features extracted from these original data channels. The theory developed during this effort should also be applicable to other areas of processing.

Finally, in the area of interpretive techniques, we have developed procedures for producing radiation balance maps from the wide spectrum covered by the new multispectral scanners. This type of map and variants of it should prove useful in agriculture, meteorology, hydrology, geography, and other disciplines in which energy budget relationships are of interest.

REFERENCES

1. Malila, W.A., R.B. Crane, & R.E. Turner, "Information Extraction Techniques", Willow Run Laboratories, Institute of Science & Tech., University of Mich., Ann Arbor, Mich., Report No. 31650-74-T, in publication.
2. Malila, W.A., R.B. Crane, & W. Richardson, "Discrimination Techniques Employing Both Reflective and Thermal Multispectral Signals", Willow Run Laboratories, Institute of Science & Tech., University of Mich., Ann Arbor, Mich., Report No. 31650-75-T, to be published.
3. Legault, R.R., "Summary of Michigan Multispectral Investigations Program", Section 37, Third Annual Earth Resources Program Review, Volume II, Dec. 1-3, 1970, NASA/MSC, Houston, Texas.
4. Nalepka, R.F., J.P. Morgenstern, & W.L. Brown, "Detailed Interpretation and Analysis of Selected Corn Blight Watch Data Sets", 4th Annual Earth Resources Program Review, NASA/MSC, Houston, Texas, 17 January 1972.
5. Thomson, F.J., "User Oriented Multispectral Data Processing at The University of Michigan", Fourth Annual Earth Resources Program Review, NASA/MSC, Houston, Texas, 17 January 1972.
6. Crane, R.B., "Preprocessing Techniques to Reduce Atmospheric and Sensor Variability in Multispectral Scanner Data", Proceedings of Seventh International Symposium on Remote Sensing of Environment, Ann Arbor, Michigan, June 1971, pp. 1345-1356.
7. Malila, W.A., R.B. Crane, C.A. Omarzu, & R.E. Turner, "Studies of Spectral Discrimination", Willow Run Laboratories, Institute of Science & Tech., University of Michigan, Ann Arbor, Mich., Report No. 31650-22-T, May 1971.
8. Turner, R.E., W.A. Malila, & R.F. Nalepka, "Importance of Atmospheric Scattering in Remote Sensing, or Everything You've Always Wanted to Know About Atmospheric Scattering But Been Afraid to Ask", Proceedings of Seventh International Symposium on Remote Sensing of Enviornment. Ann Arbor, Mich., June 1971, pp. 1651-1698.
9. Suits, G.H., G. Safir, & A. Ellingboe, "Prediction of Directional Reflectance of a Corn Field Under Stress", Fourth Annual Earth Resources Program Review, NASA/MSC, Houston, Texas, 17 January 1972.

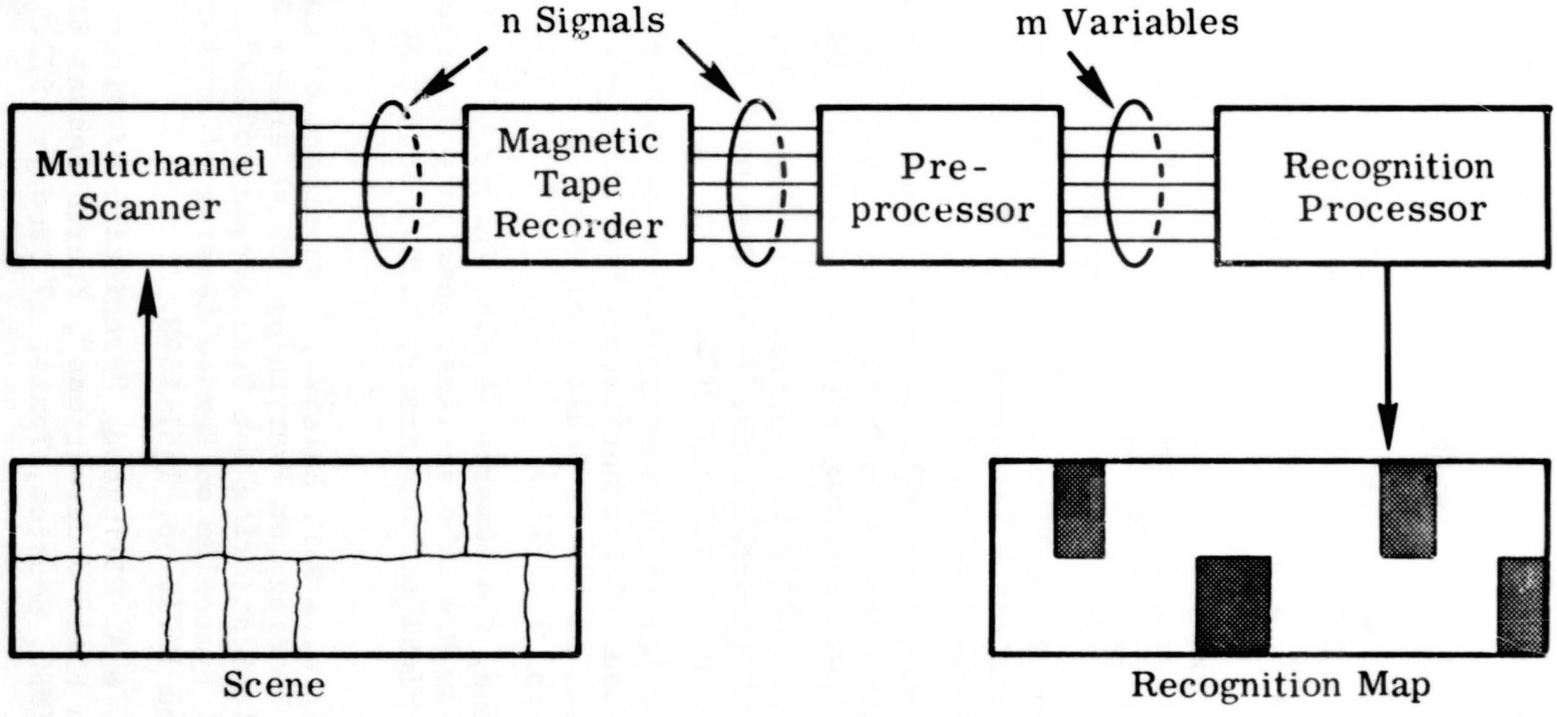

FIGURE 1. MULTISPECTRAL REMOTE SENSING AND PROCESSING SYSTEM

CLASS	SYSTEMATIC	RANDOM
Atmosphere	Path length Geometry	Inhomogeneities Clouds
Sun Position	Time, Date Location	
Scan Geometry	Nadir angle Azimuth w.r.t. sun Altitude	Angle errors Terrain profile
Sensor	Aperture effects Gain changes	System noise

FIGURE 2. SOURCES OF VARIATIONS IN MULTISPECTRAL SCANNER SIGNALS

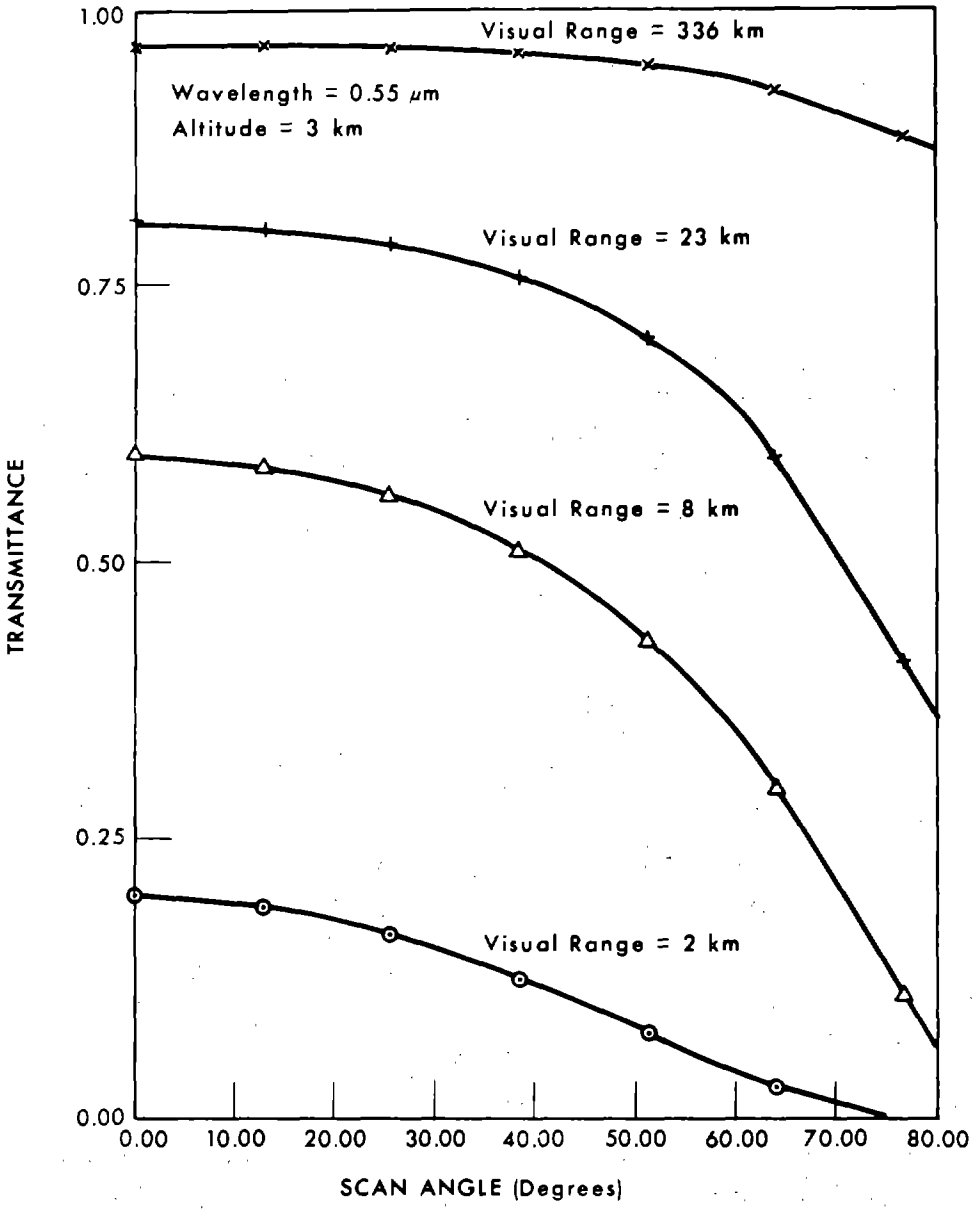

FIGURE 3. DEPENDENCE OF TRANSMITTANCE ON NADIR SCAN ANGLE FOR VARIOUS VISUAL RANGES

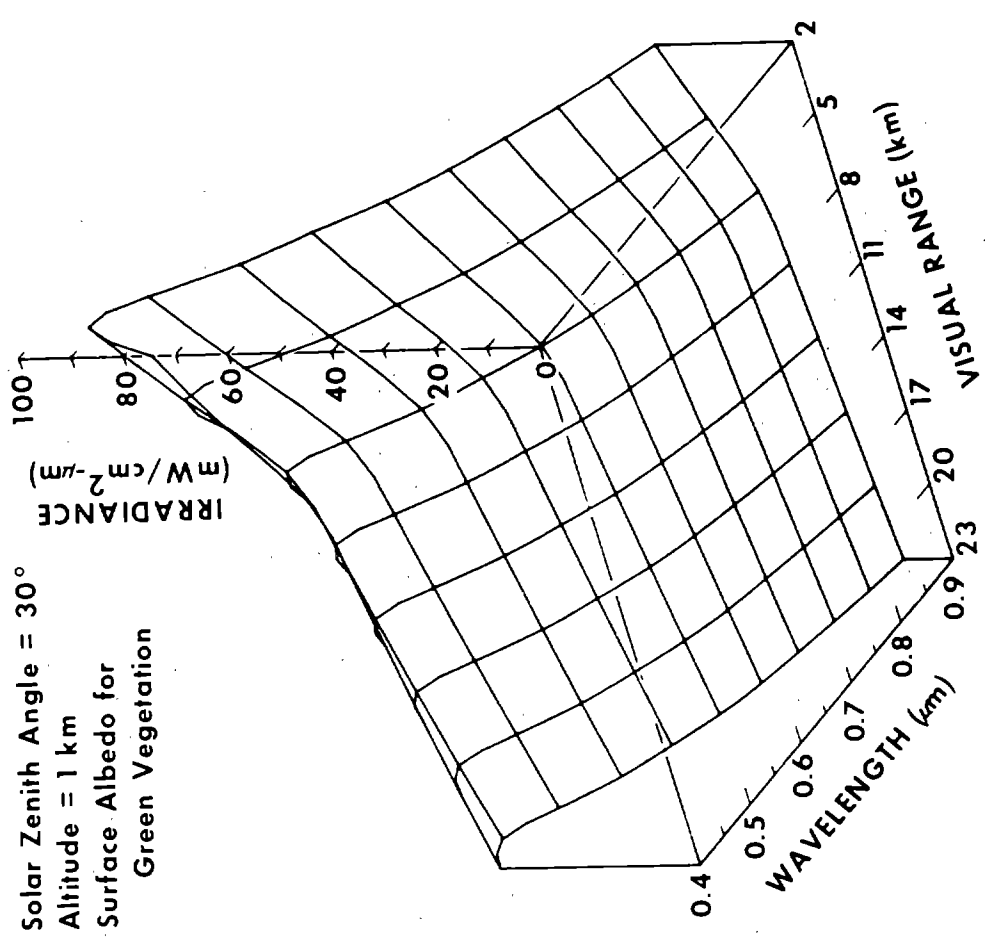

FIGURE 4. DEPENDENCE OF DIFFUSE DOWNWARD IRRADIANCE ON VISUAL RANGE AND WAVELENGTH

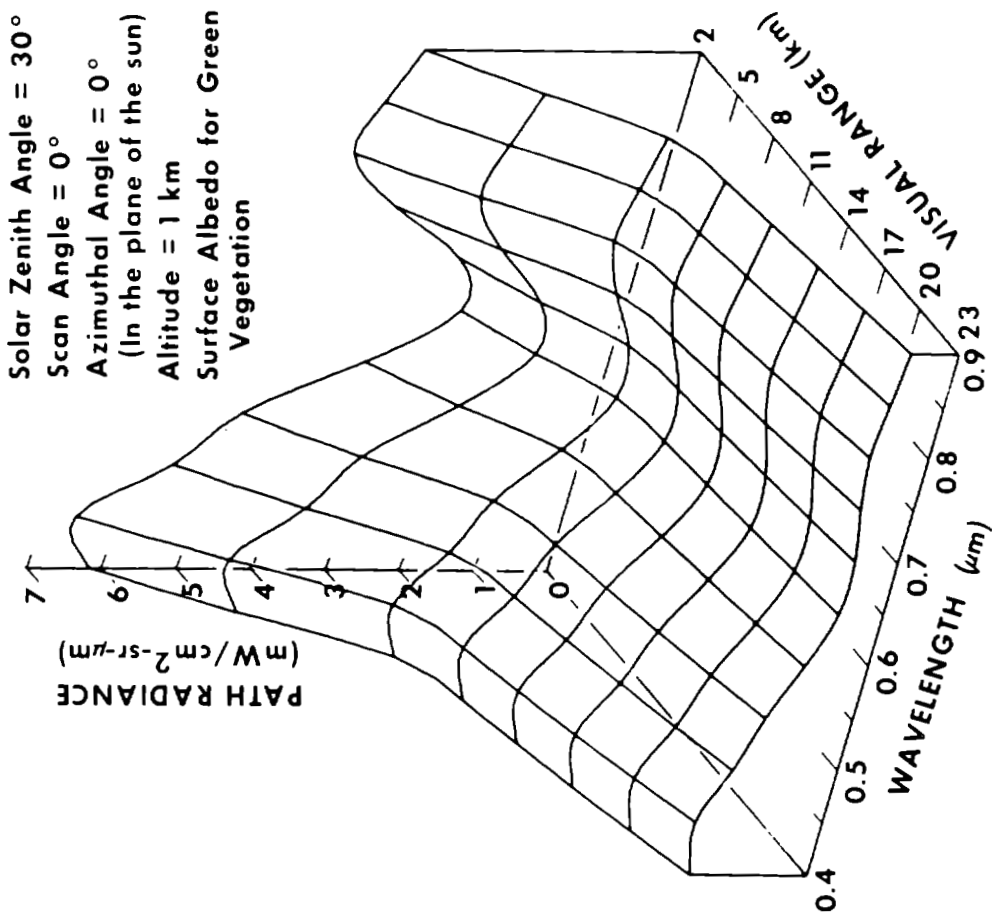

FIGURE 5. DEPENDENCE OF PATH RADIANCE ON VISUAL RANGE AND WAVELENGTH

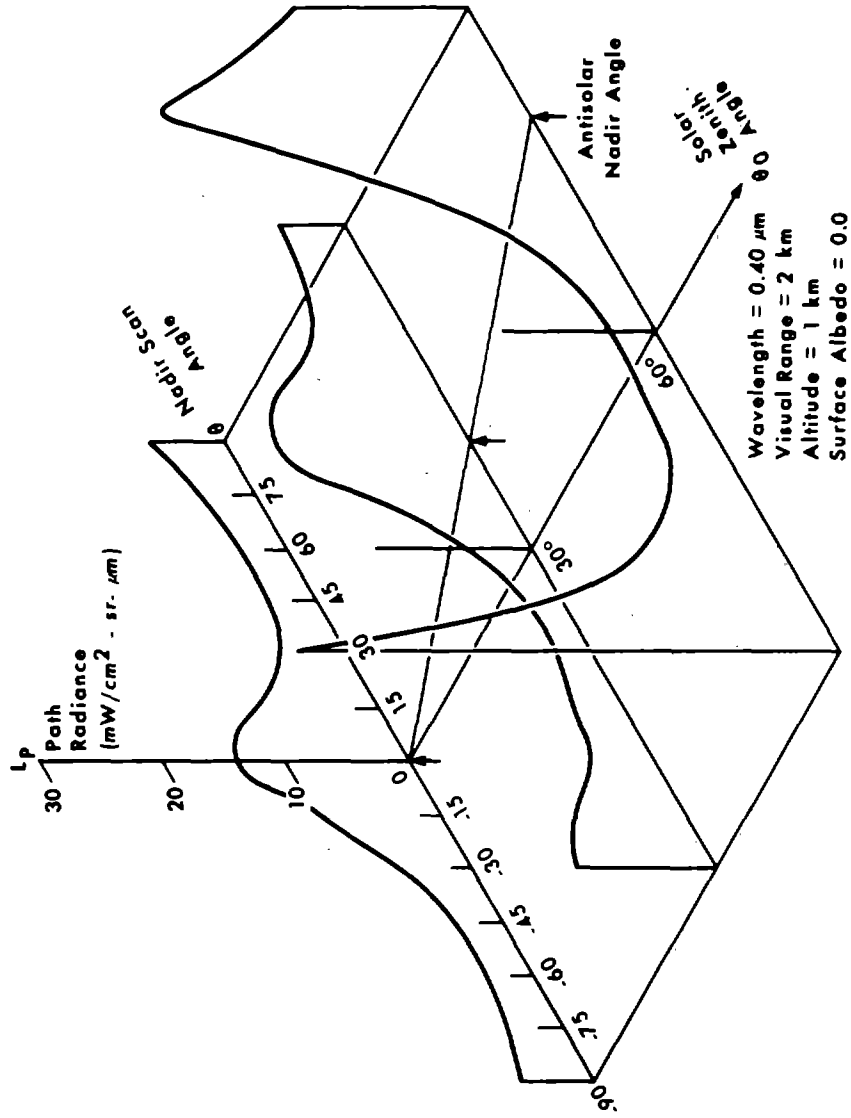

FIGURE 6. PATH RADIANCE VERSUS SCAN ANGLE AND SOLAR ZENITH ANGLE

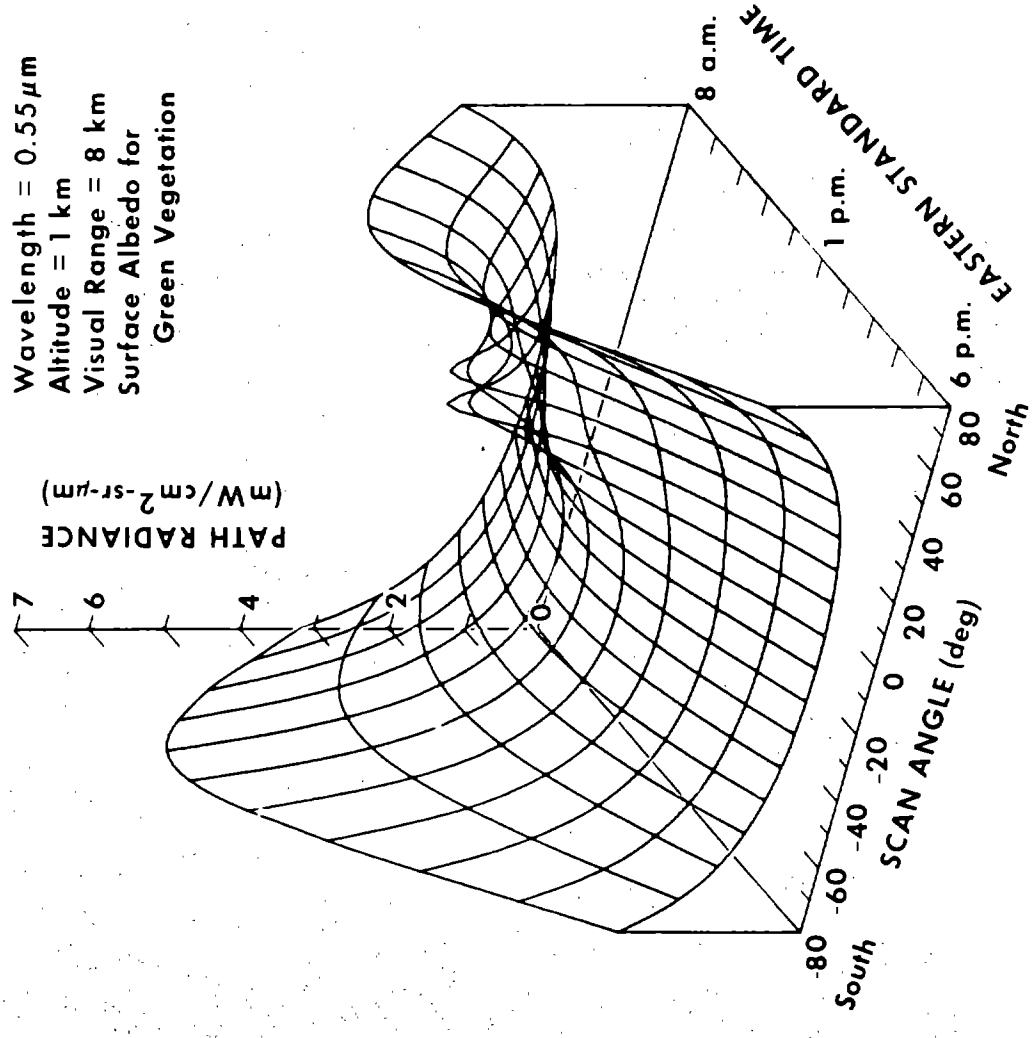

FIGURE 7. DEPENDENCE OF PATH RADIANCE ON TIME AND SCAN ANGLE. Southeastern Michigan, 1 September 1971.

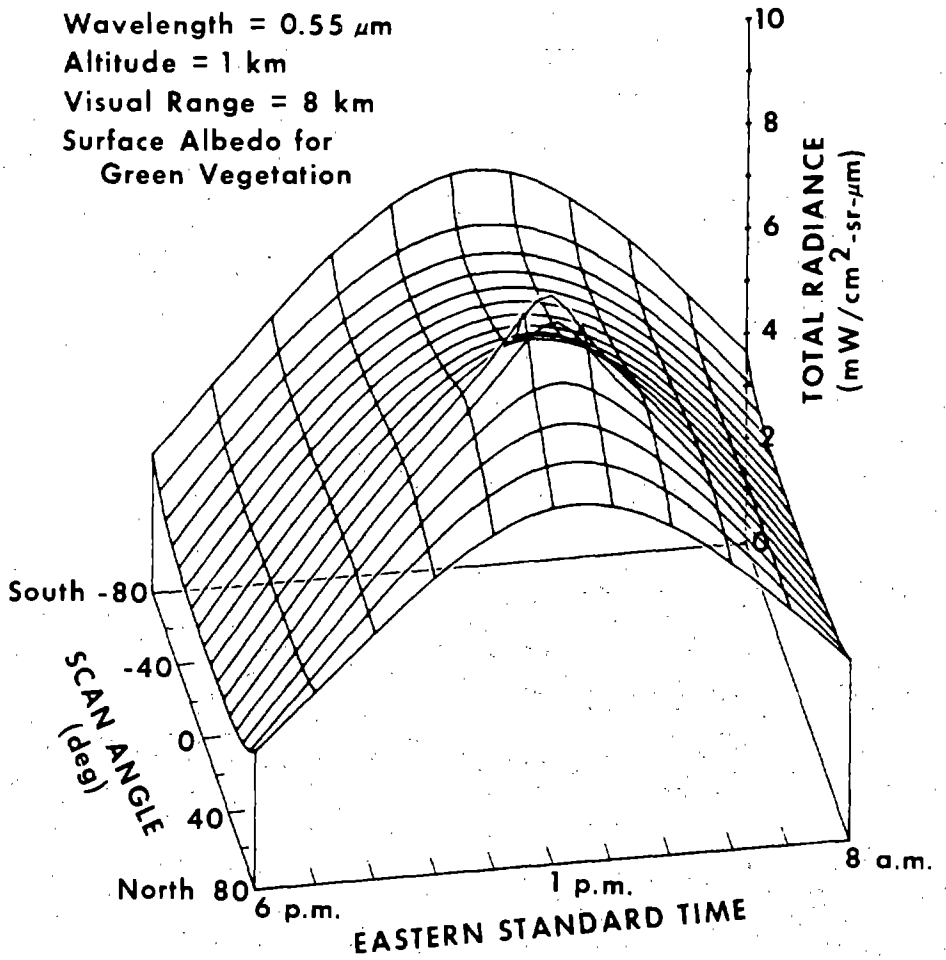

FIGURE 8. DEPENDENCE OF TOTAL RADIANCE ON TIME AND SCAN ANGLE. Southeastern Michigan, 1 September 1971

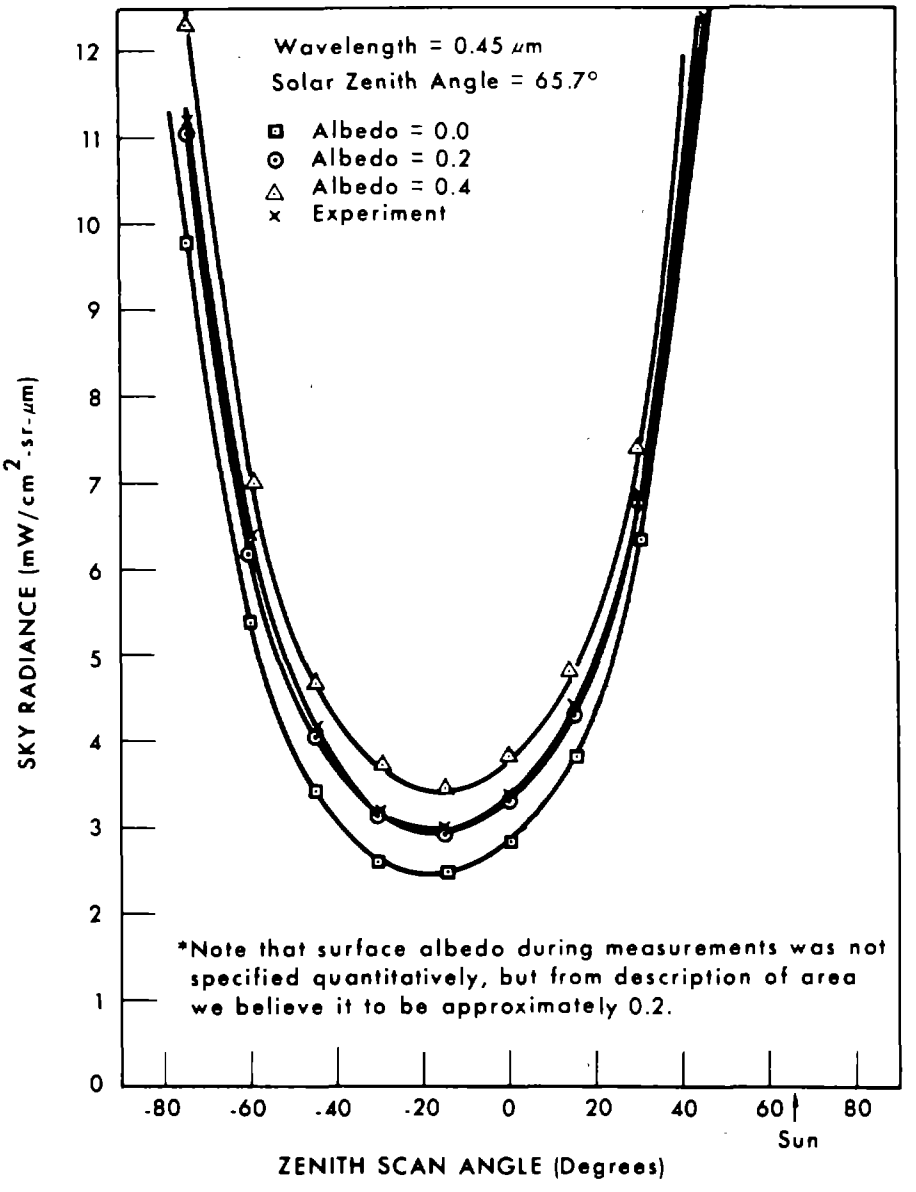

FIGURE 9. DEPENDENCE OF SKY RADIANCE ON ZENITH ANGLE IN SOLAR PLANE FOR CLEAR SKY CONDITIONS

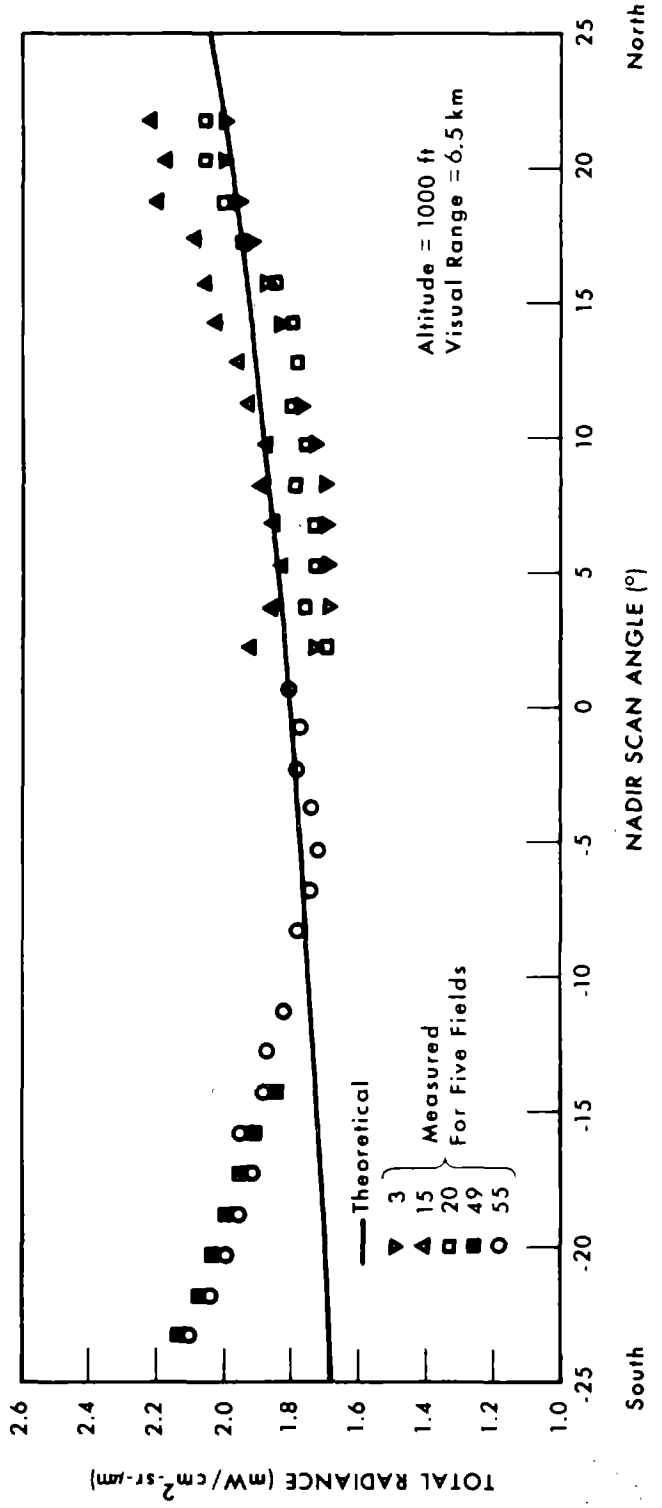

FIGURE 10. COMPARISON OF CALCULATED AND MEASURED RADIANCE DATA FOR SOYBEAN FIELDS (WAVELENGTH OF 0.42 μm)

C.2

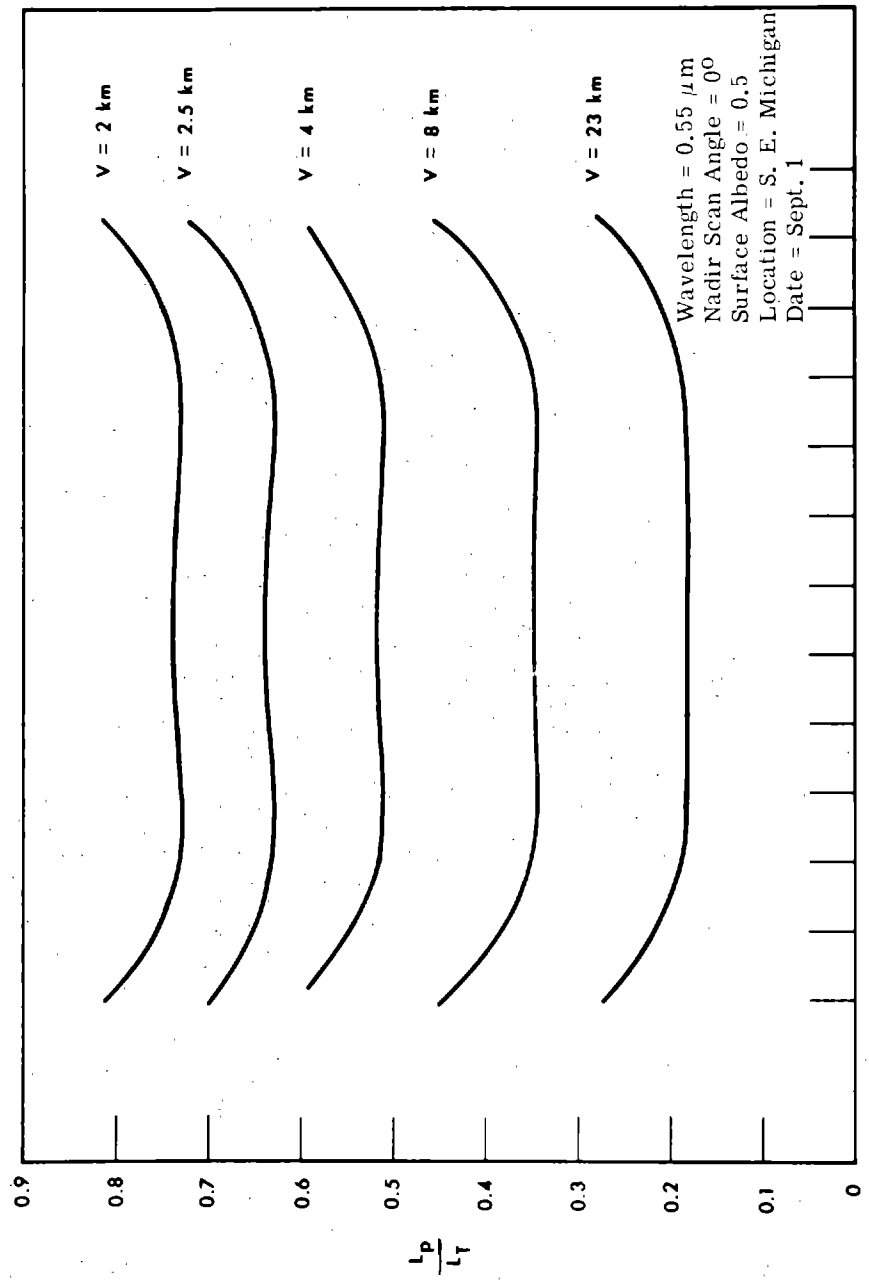

FIGURE 11. RATIO OF PATH RADIANCE TO TOTAL RADIANCE AT AN ALTITUDE OF 5 km AS A FUNCTION OF TIME

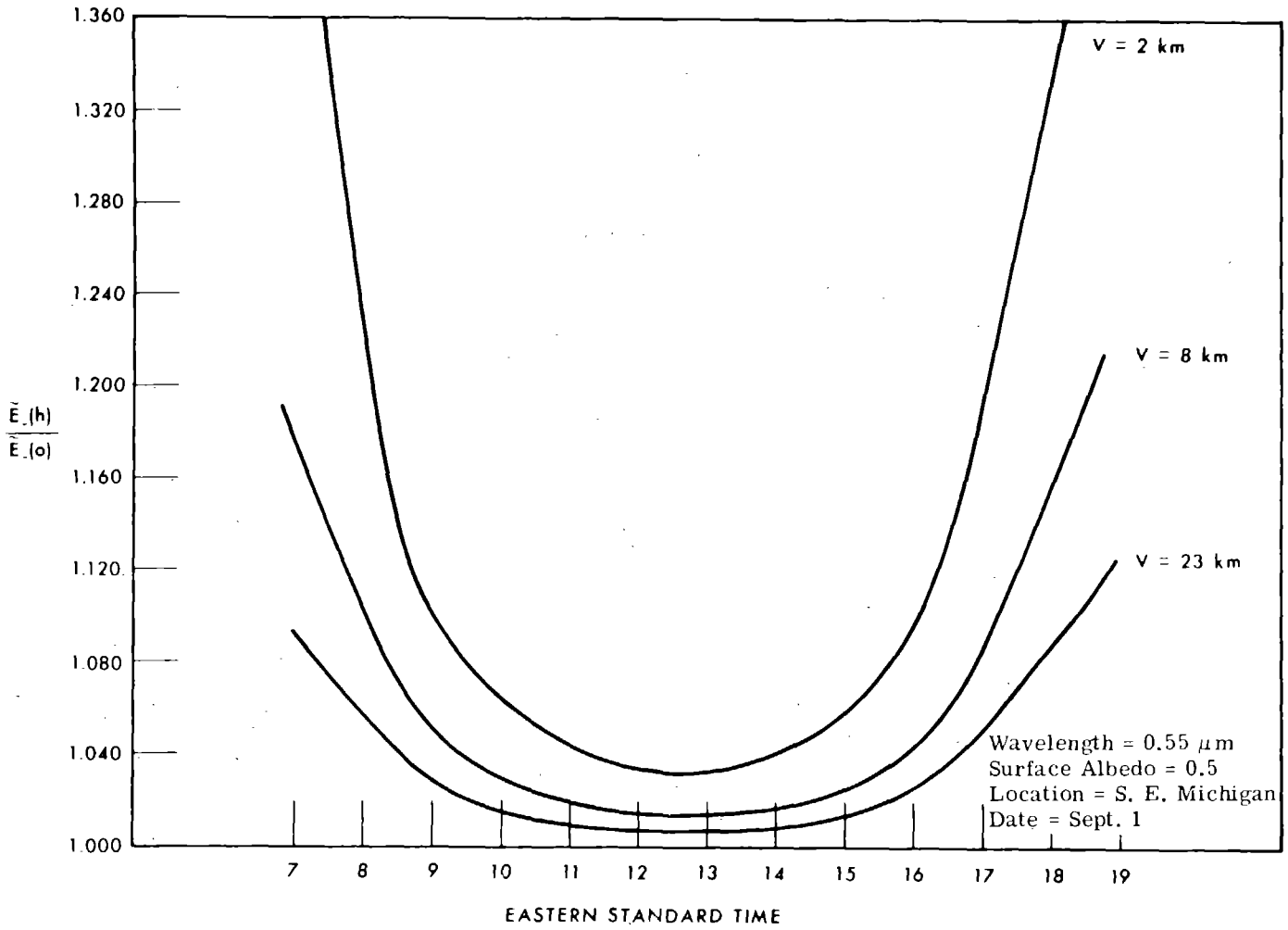

FIGURE 12. RATIO OF TOTAL DOWNWARD IRRADIANCE AT AN ALTITUDE OF 5 km TO TOTAL DOWNWARD IRRADIANCE AT EARTH'S SURFACE AS A FUNCTION OF TIME

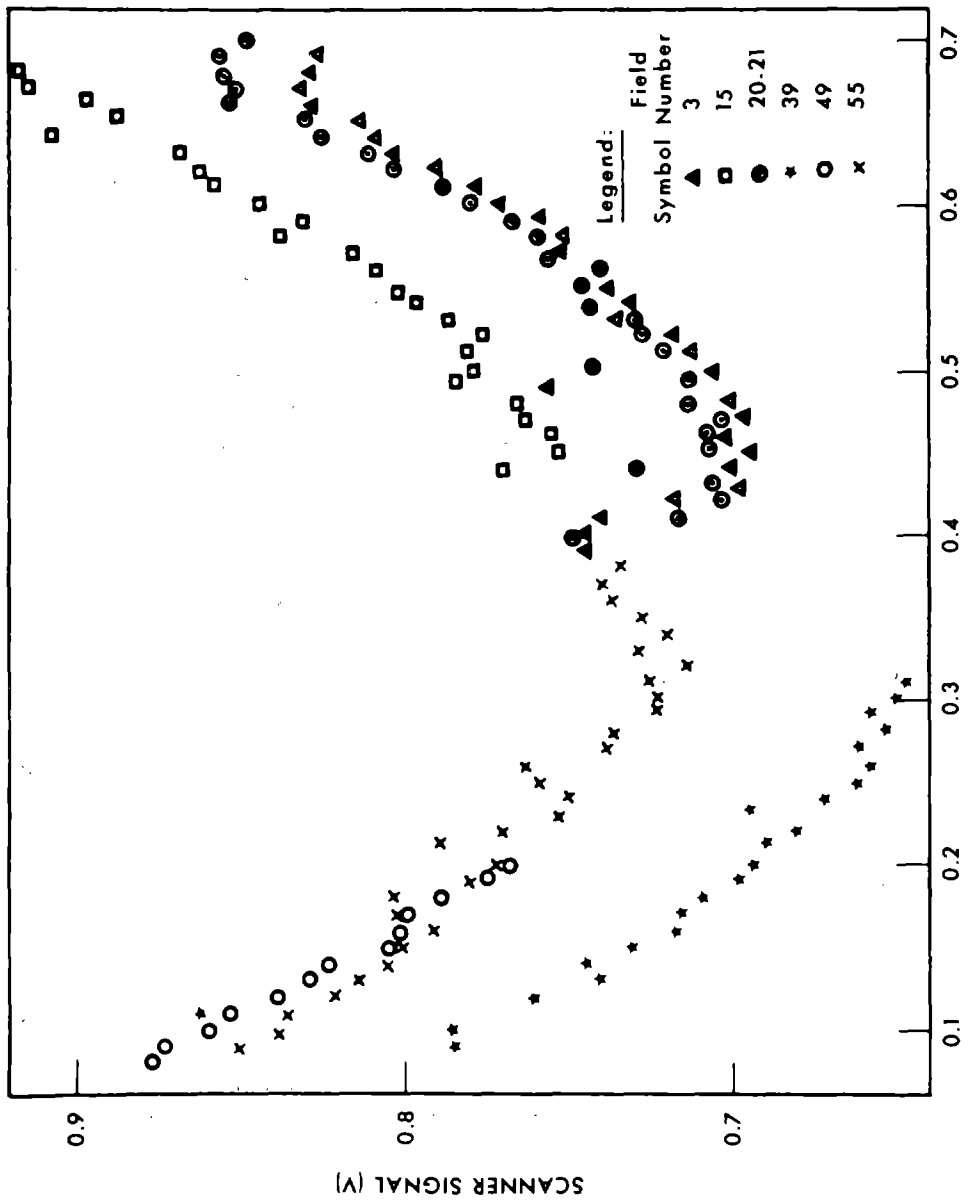

FIGURE 13. SCAN ANGLE EFFECT IN 6 SOYBEAN FIELDS (UNCORRECTED)

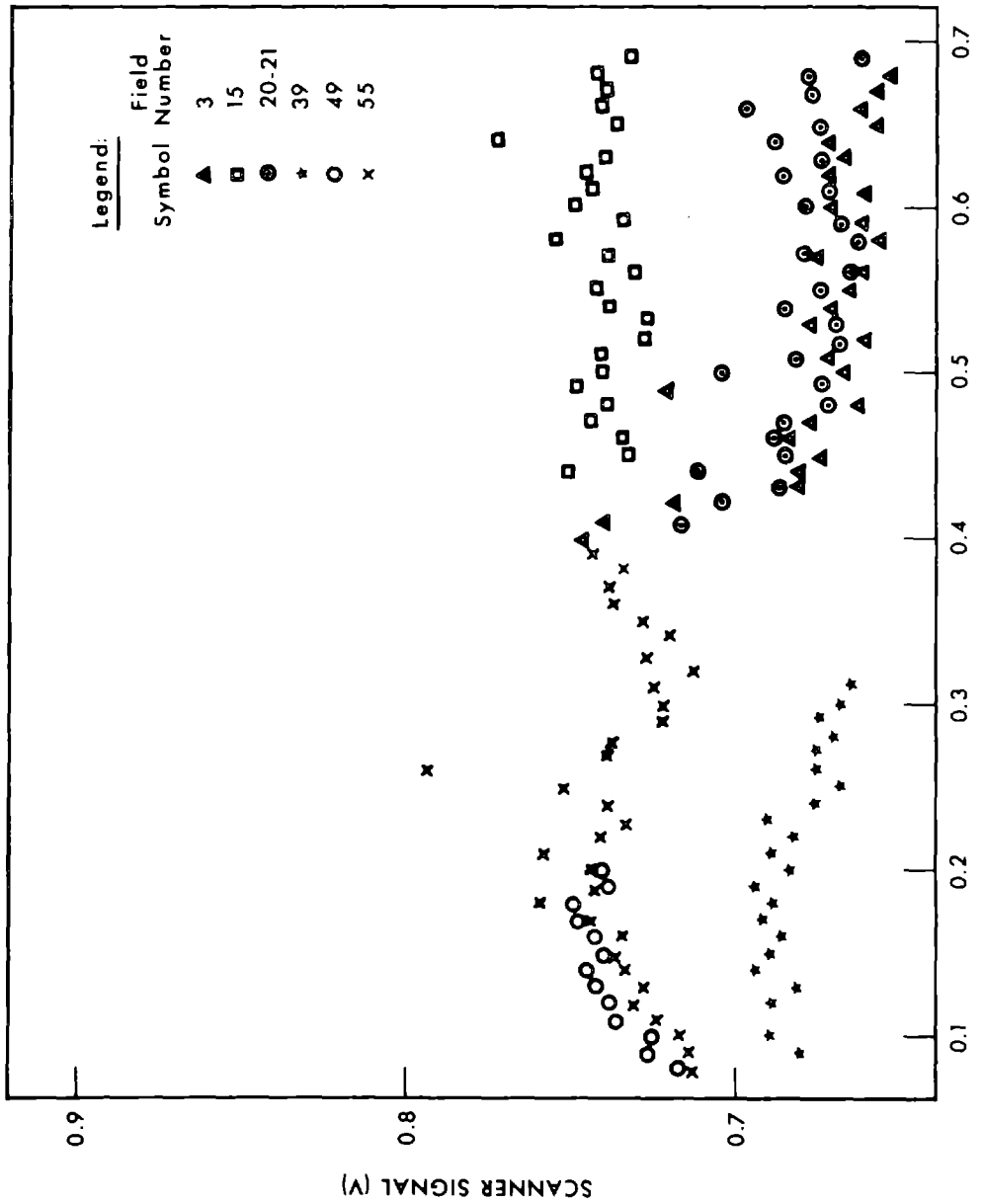

FIGURE 14. SCAN ANGLE EFFECT IN 6 SOYBEAN FIELDS AFTER QUADRATIC UV CORRECTION

Data Description					
ALTITUDE	1Kft	1Kft	1Kft	5Kft	5Kft
SMOOTHING	--	Yes	Yes	--	Yes
PREPROCESSING	--	--	U-V	--	U-V
TRAINING ALT.	1Kft	1Kft	1Kft	5Kft	1Kft
Pct. Fields with Pcorrect < 0.5	48	45	24	48	45
Percent Fields with Majority Decision Incorrect	14	14	3	24	17

FIGURE 15. COMPARISON OF RECOGNITION RESULTS

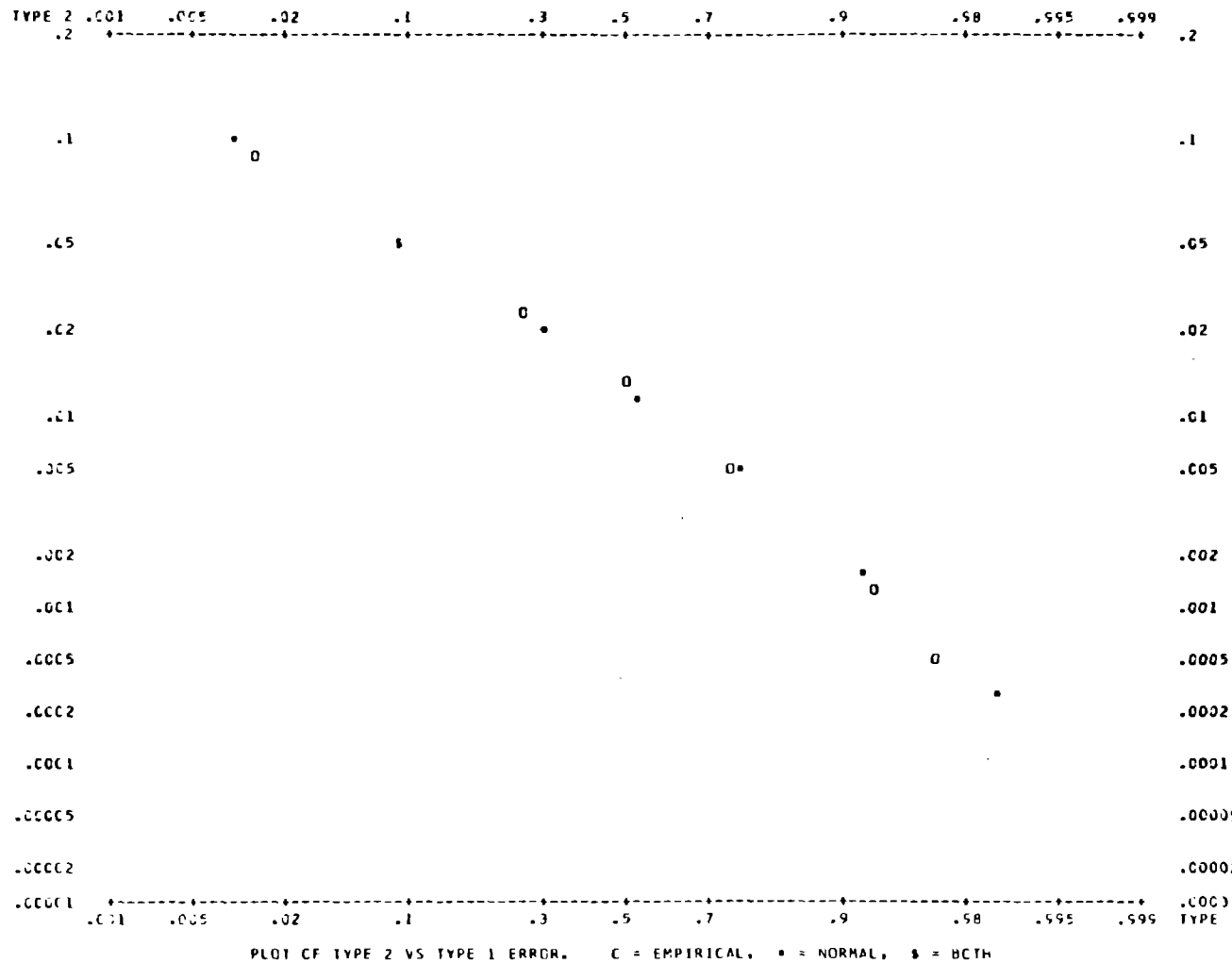

FIGURE 16. EFFECT OF LIKELIHOOD FUNCTION ON OPERATING CHARACTERISTICS (TYPICAL FOR THE FIRST THREE VARIABLES)

- Criterion is average expected loss (probability of misclassification)
- Stepwise procedure
- New linear approximation is 50 times faster than quadratic method

FIGURE 17. FEATURES OF CHANNEL SELECTION PROCEDURE

QUADRATIC METHOD (1 HOUR)

Channel Order	4	10	1	9	7	5
Avg. Prob. Miscl.	0.119	0.054	0.031	0.025	0.023	0.021

LINEAR METHOD (70 Sec)

Channel Order	4	10	1	9	7	5
Avg. Prob. Miscl.	0.122	0.059	0.034	0.028	0.025	0.024

FIGURE 18. COMPARISON OF CHANNEL SELECTION PROCEDURES
(9 signatures, 10 data channels)

$$R_N = ET + H + S + P$$

where

R_N is Net Incoming Radiant Energy

ET is Energy for Evapotranspiration

H is Energy for Heating Air (Sensible Heat)

S is Energy Conducted (e.g., Soil Heat Flux)

P is Net Energy Conversion (Photosynthesis minus respiration for Plants)

FIGURE 19. ENERGY BUDGET

$$E_{net} = (1 - \rho)E_S + \epsilon E_L - M_L$$

where

E_{net} is Net Irradiance
(Net Incoming Radiant Power Density)

E_S is Irradiance at Short Wavelengths
(Direct Sunlight + Skylight)

ρ is Reflectance of Surface (Albedo)

E_L is Irradiance at Long Wavelengths
(Incoming Thermal Radiation)

ϵ is Thermal Emittance of Surface

M_L is Exitance at Long Wavelengths
(Emitted Thermal Radiation)

Typical Units: watts/m^2

cal - cm^{-2}/min = ly/min

FIGURE 20. RADIATION BALANCE

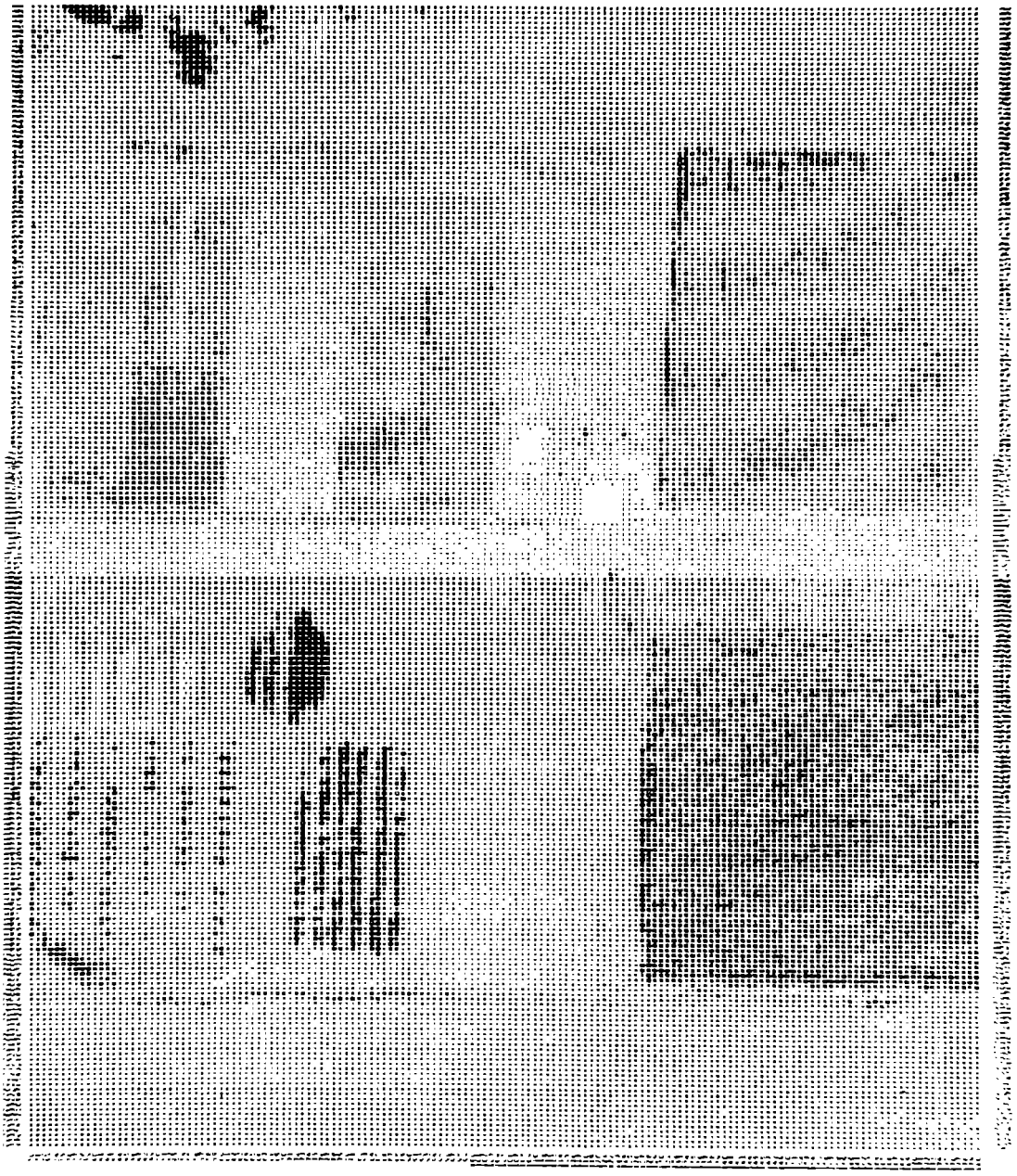

FIGURE 21. EXAMPLE EXITANCE MAP

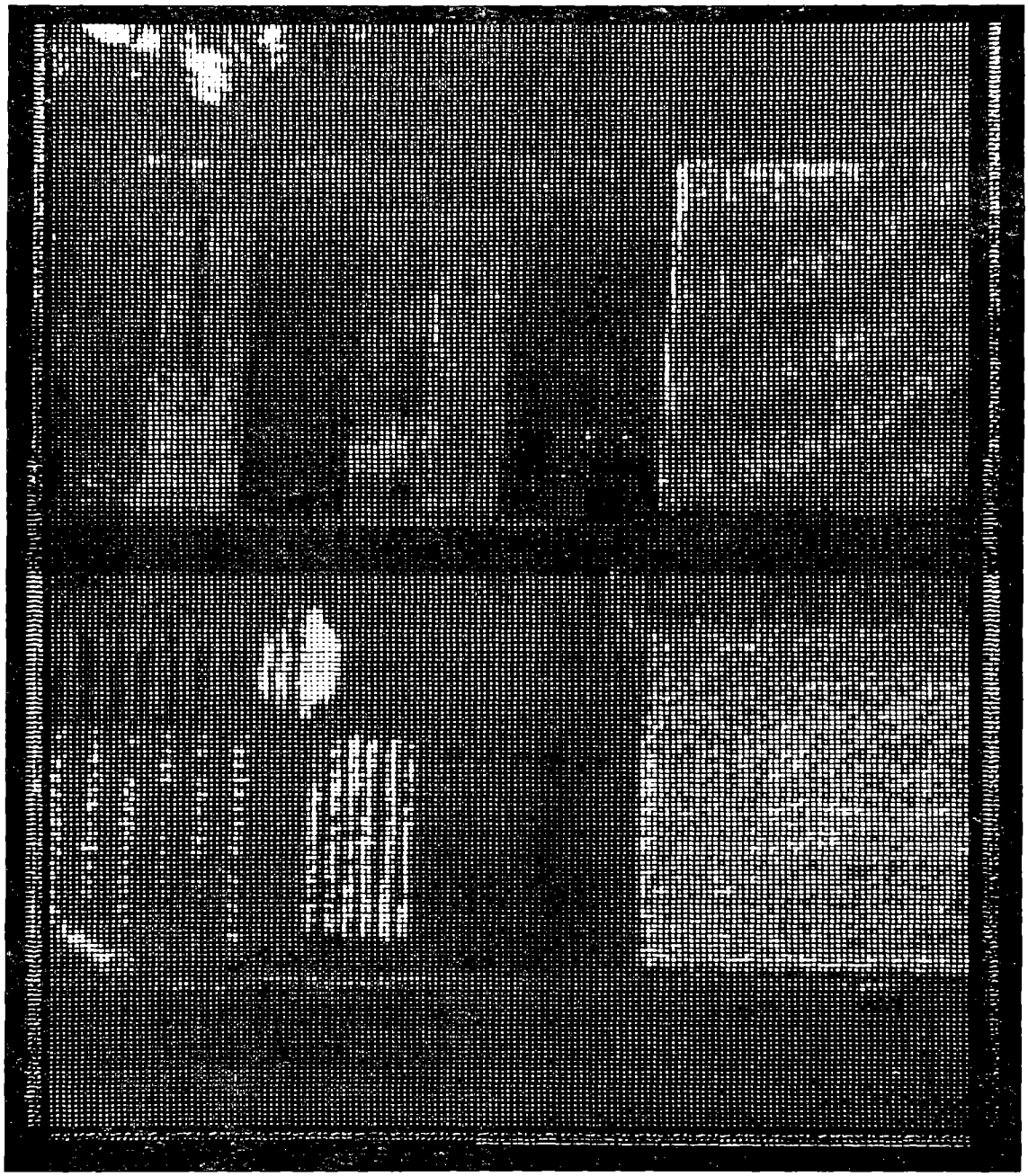

FIGURE 22. EXAMPLE RADIATION BALANCE MAP